

Supporting Information

Tailoring Desolvation Kinetics Enables Stable Zinc Metal Anodes

Zhen Hou,^a Hong Tan,^a Yao Gao,^a Menghu Li,^b Ziheng Lu^{*b} and Biao Zhang^{*a}

^a Department of Applied Physics, the Hong Kong Polytechnic University, Hung Hom, Kowloon, Hong Kong, P.R. China

^b Shenzhen Institutes of Advanced Technology, Chinese Academy of Sciences, Shenzhen 518055, P.R. China

E-mail: biao.ap.zhang@polyu.edu.hk (Biao Zhang); E-mail: zh.lu1@siat.ac.cn (Ziheng Lu)

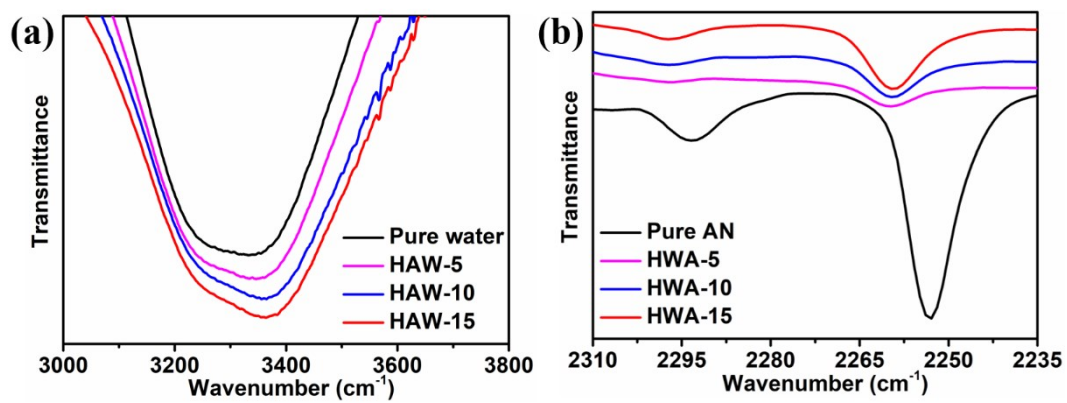


Figure S1. (a) IR spectra of the O–H stretching vibration of water molecules in pure water and HWAs; (b) IR spectra of the C≡N stretching vibration in pure AN and HWAs.

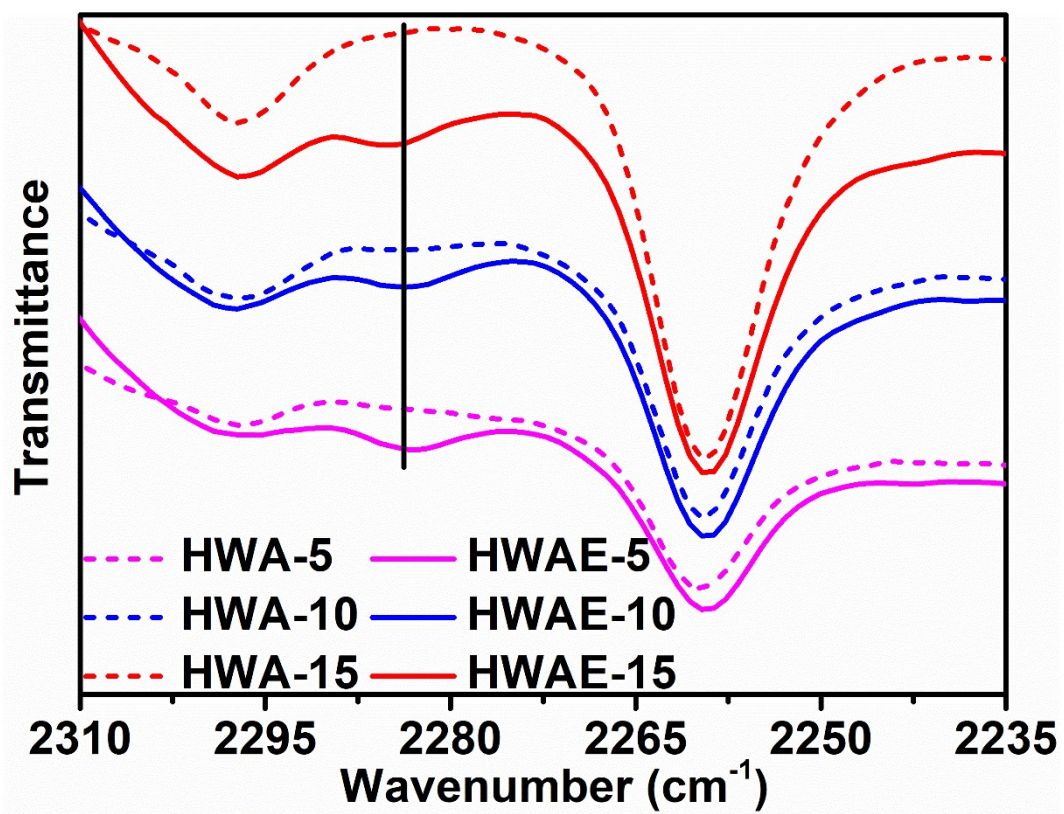


Figure S2. IR spectra of the C≡N stretching vibration in HWAs and HWAEs.

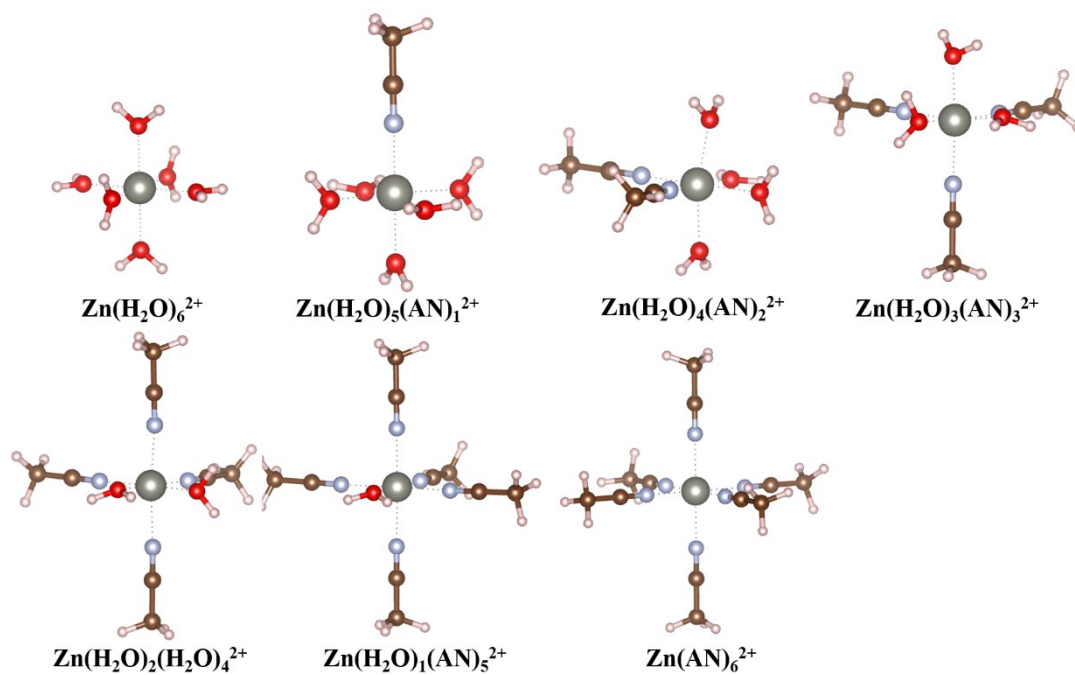


Figure S3. Structures of the most stable $\text{Zn}(\text{H}_2\text{O})_x(\text{AN})_{6-x}^{2+}$ complexes.

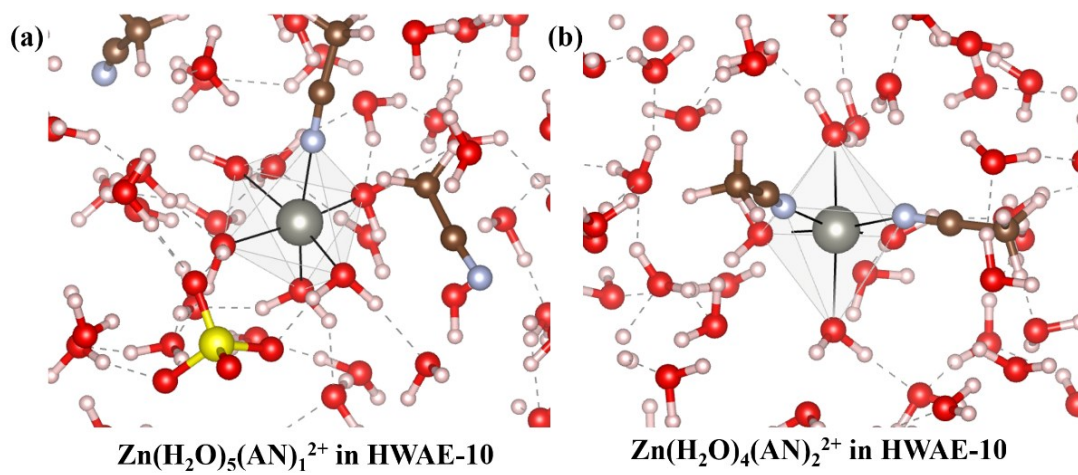


Figure S4. Snapshots of the AIMD simulations of HWAE-10.

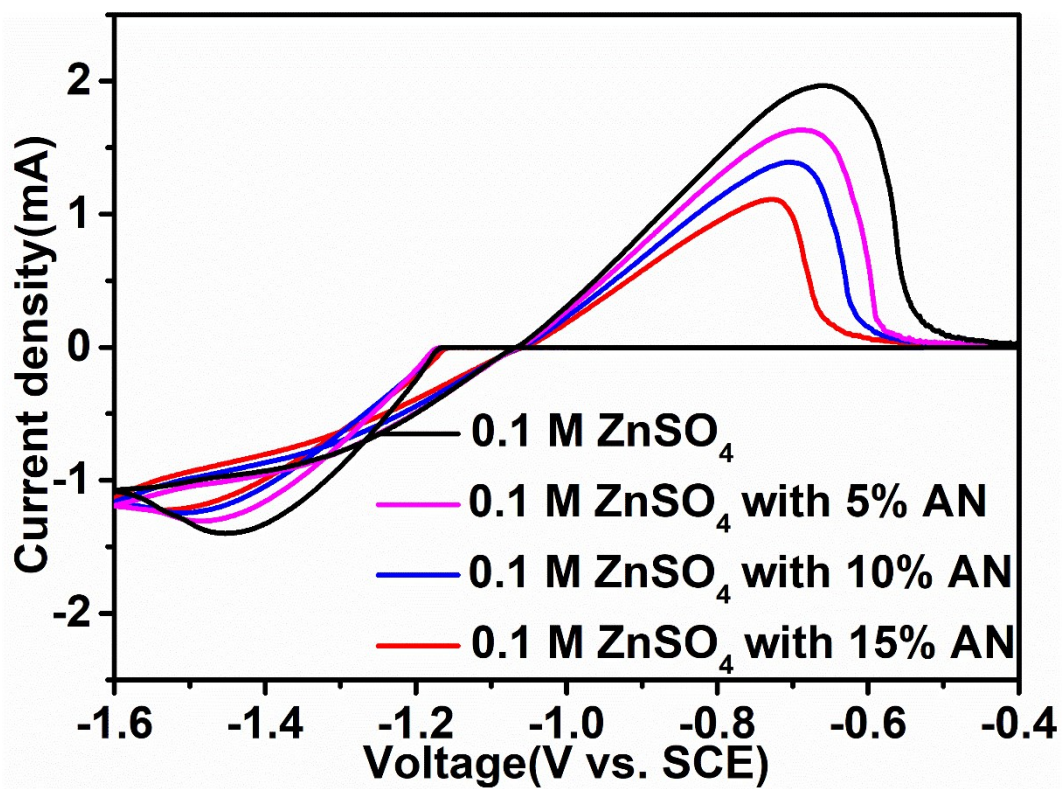


Figure S5. CV at a scan rate of 20 mV/s in 0.1 M ZnSO₄ with/without AN.

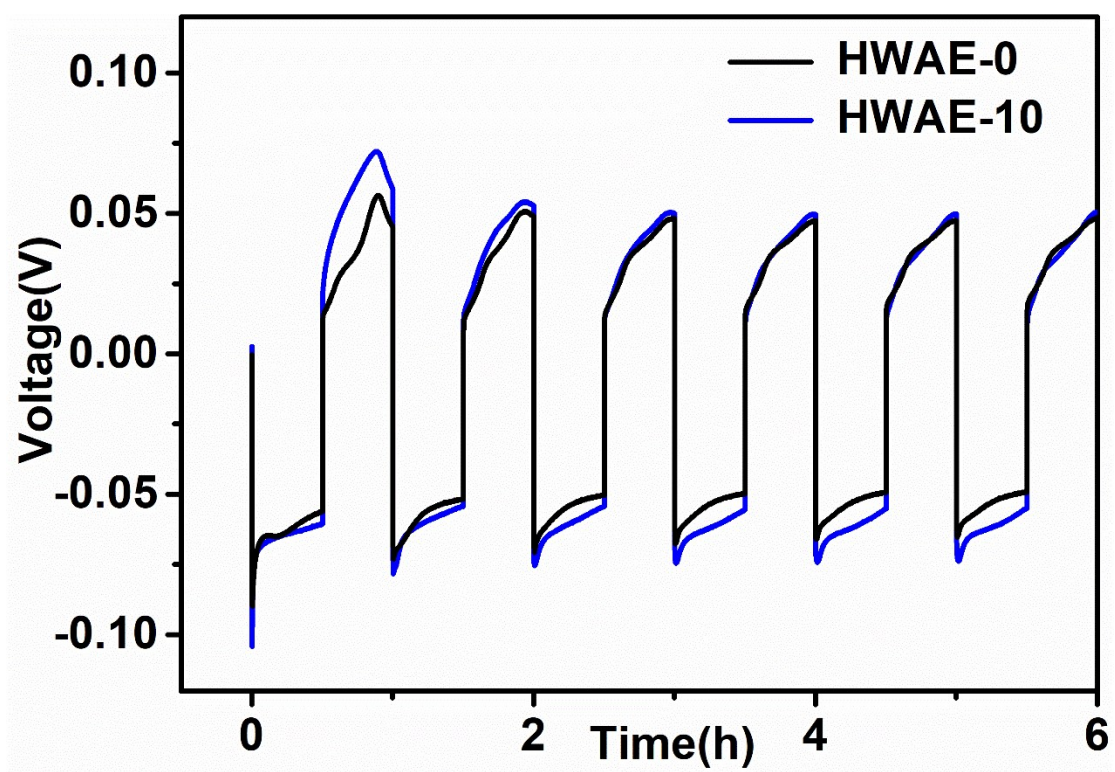


Figure S6. Cycling performances using three electrodes system with Zn foil as the working/counter/reference electrodes at 2 mA/cm² in HWAE-0 and HWAE-10.

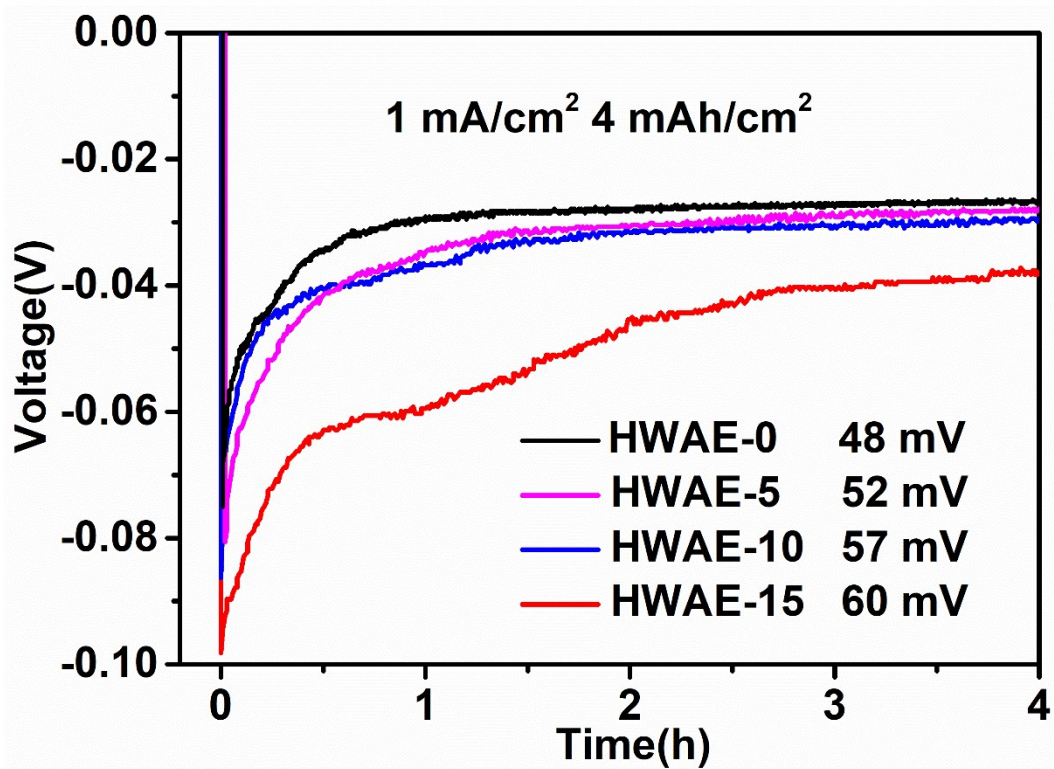


Figure S7. Nucleation overpotentials using Zn/Cu cells in HWAEs.

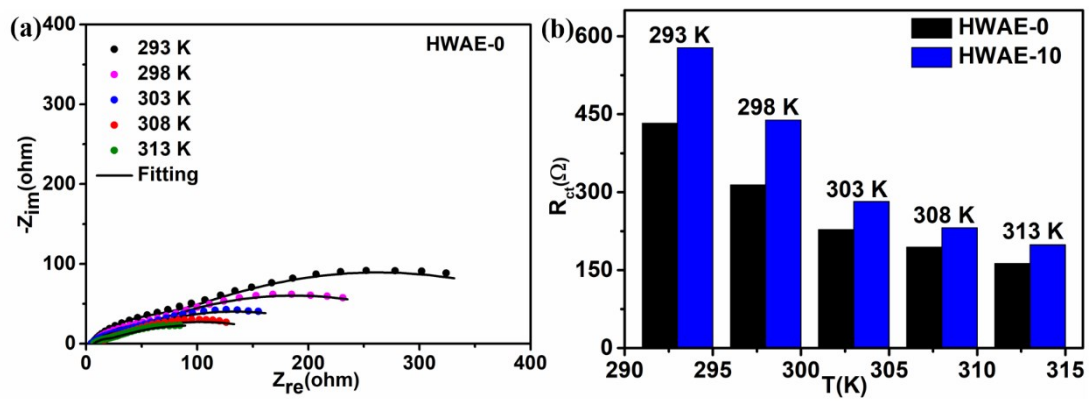


Figure S8. (a) Nyquist plots at different temperatures using Zn/Cu cells in HWAE-0; (b) Fitted values of R_{ct} from Nyquist plots.

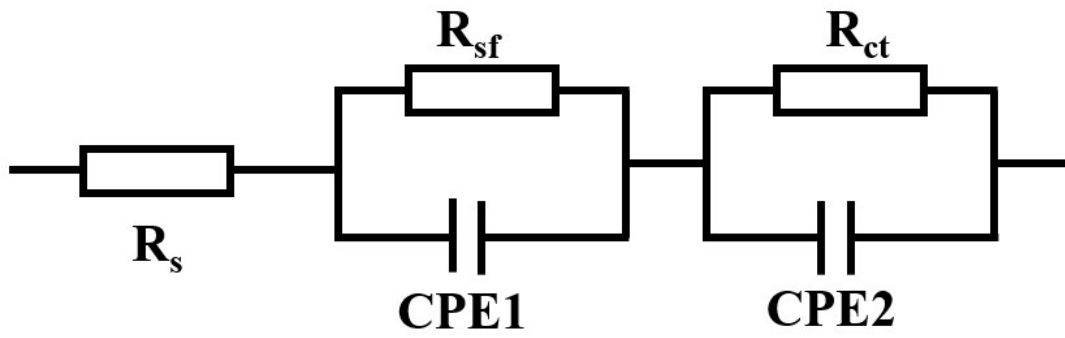


Figure S9. Equivalent circuit model for EIS plots using Zn/Cu cells in HWAE-0 and HWAE-10.

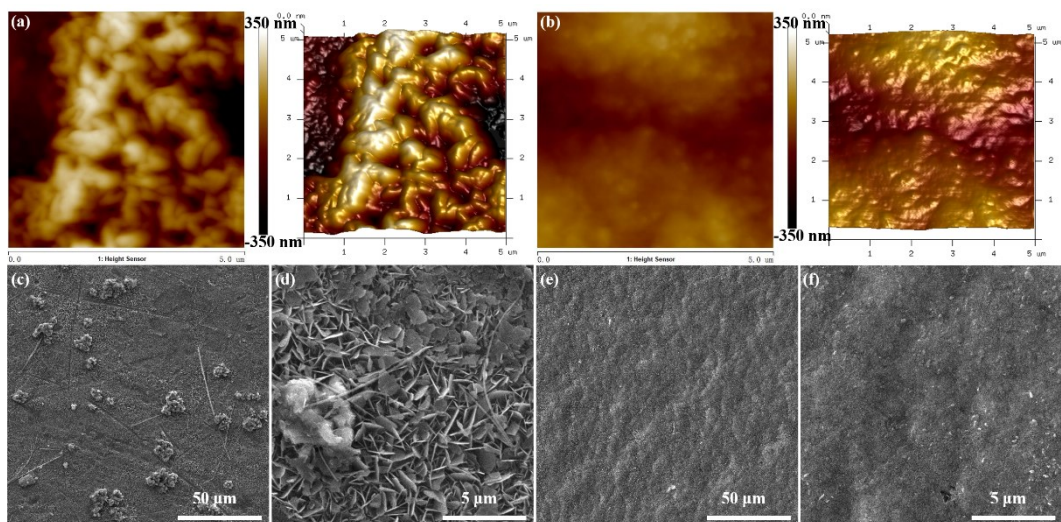


Figure S10. AFM images of Zn deposition on Cu current collector with 0.2 mAh/cm^2 (720 s) at 1 mA/cm^2 in (a) HWAE-0 and (b) HWAE-10; Corresponding SEM images in (c, d) HWAE-0 and (e, f) HWAE-10.

Atomic force microscopy (AFM) images show a rough surface of Zn is deposited in HWAE-0 as a reflection of non-uniform nucleation, while Zn deposition shows a smoother texture in HWAE-10. The average surface roughness (R_a) of deposited Zn in HWAE-10 is 49.4 nm, which is much lower than 100 nm in HWAE-0, suggesting AN addition is beneficial to regulate Zn growth.

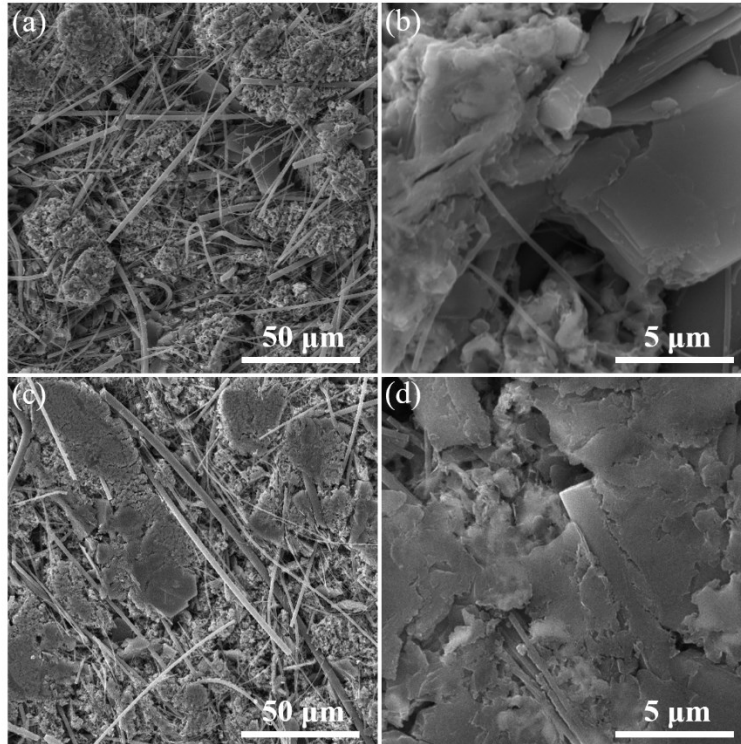


Figure S11. SEM images of Zn deposition on Cu current collector with 4 mAh/cm² (14400 s) at 1 mA/cm² in (a, b) HWAE-0 and (c, d) HWAE-10.

Regarding the formation of zinc dendrites in HWAE-0:

Both Zn²⁺ and electric fields tend to concentrate on the protuberances with high surface energy. Therefore, the zinc nucleation and growth prefer to occur at this tip (i.e., “tip effect”) during the deposition process, which leads to inhomogeneous Zn deposition. The formed Zn protuberances further increase the local electric field intensity around them, leading to the growth of Zn protuberances into Zn dendrites upon cycling. The Zn dendrites finally pierce the separator and cause internal short circuits.

In HWAE-10, the supersaturation of adatoms is realized between the electrode/electrolyte interfaces. Thus, numerous Zn nuclei will be produced for the homogenous Zn growth, suppressing the “tip effect”.

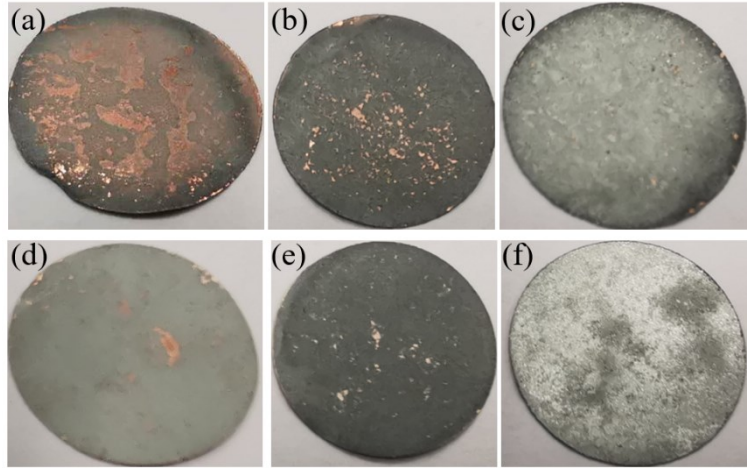


Figure S12. Optical photos of Zn deposition on Cu current collector at 1 mA/cm^2 with 1 mAh/cm^2 in (a) HWAE-0 and (d) HWAE-10 and with 4 mAh/cm^2 in (b) HWAE-0 and (e) HWAE-10; After 50 cycles at 2 mA/cm^2 with a cycling capacity of 2 mAh/cm^2 in (c) HWAE-0 and (f) HWAE-10.

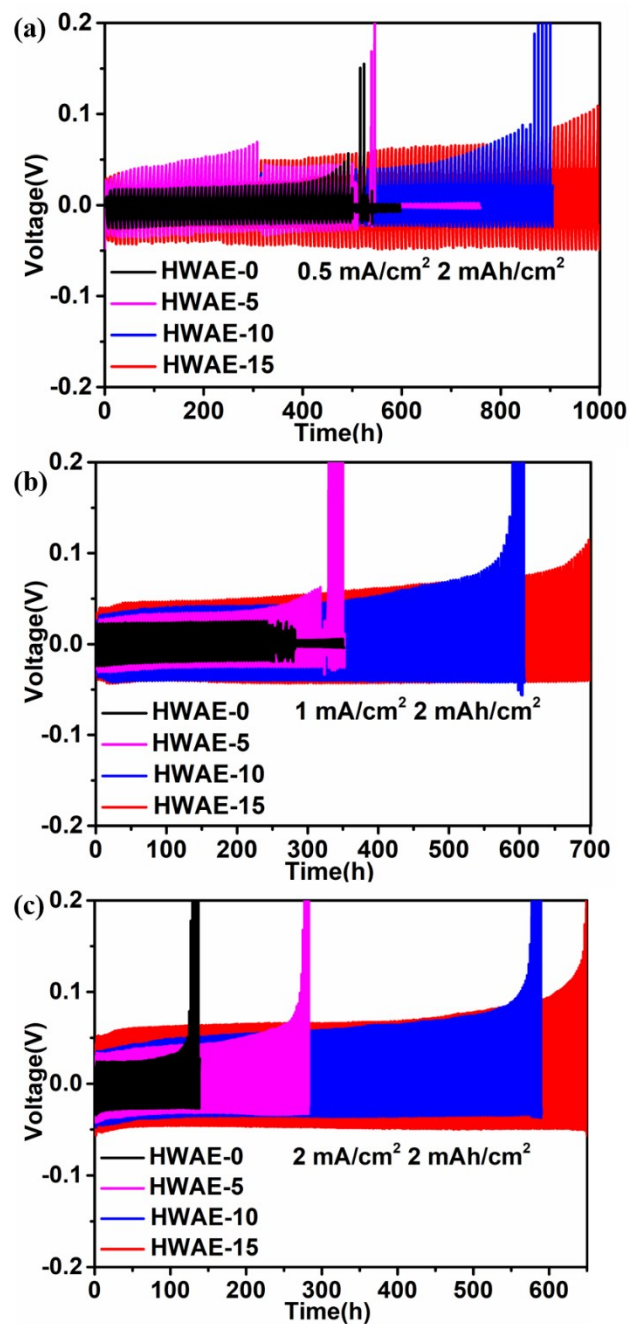


Figure S13. The cycling performances of Zn/Cu cells in HWAEs at 0.5, 1 and 2 mA/cm² with a cycling capacity of 2 mAh/cm².

Noteworthy, the short circuit accounts for the failure of Zn/Cu cells at 0.5 and 1 mA/cm² in HWAE-0, while the increased voltage polarization is responsible for the degradation at 2 mA/cm² in HWAE-0. A high depth of discharge (DOD) of 50% is

employed in the cycling test. Therefore, only limited Zn source is deposited on the Cu current collector. At a high current density of 2 mA/cm^2 , more rampant Zn dendrites with a high specific surface lead to the severe side reactions, which consume the active Zn faster than that under low current density. This will deplete the finite Zn rapidly on the Cu current collector before the evolutive Zn dendrites could pierce the separator. Therefore, increased voltage polarization is responsible for the failure at a high current density of 2 mA/cm^2 instead of a short circuit.

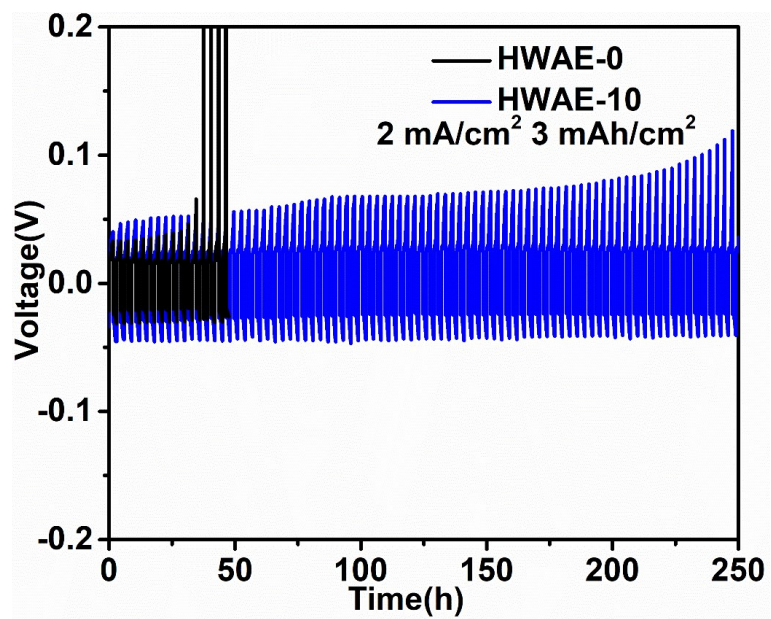


Figure S14. The cycling performances of Zn/Cu cells in HWAE-0 and HWAE-10 at 2 mA/cm² with a cycling capacity of 3 mAh/cm² (corresponds to 75% DOD).

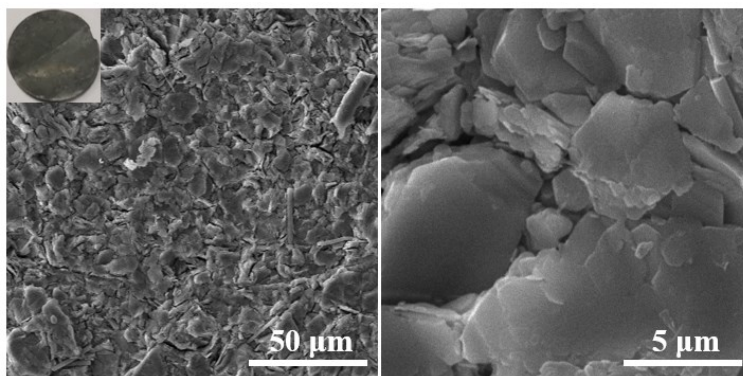


Figure S15. SEM images and optical photo of Zn after 200 cycles at 2 mA/cm² with a cycling capacity of 2 mAh/cm² in HWAE-10.

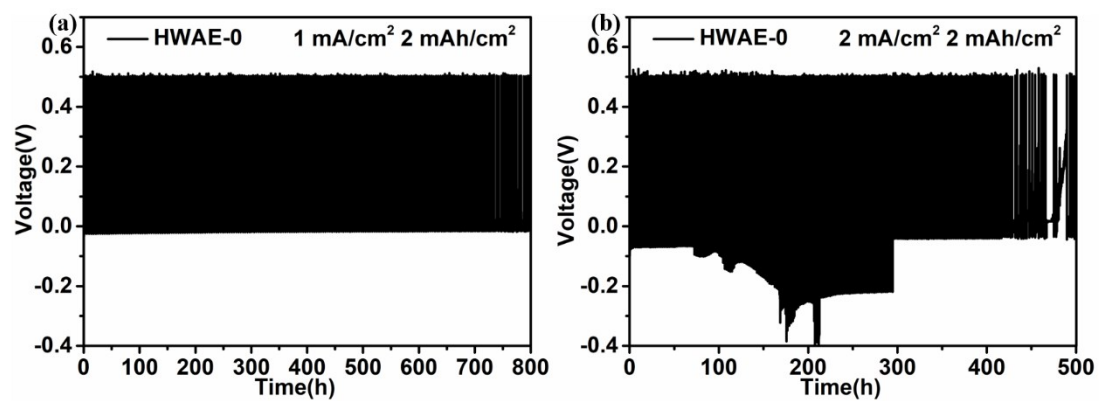


Figure S16. Time-voltage curves of CE in HWAE-0 at (a) 1 mA/cm² and (b) 2 mA/cm² with a cycling capacity of 2 mAh/cm².

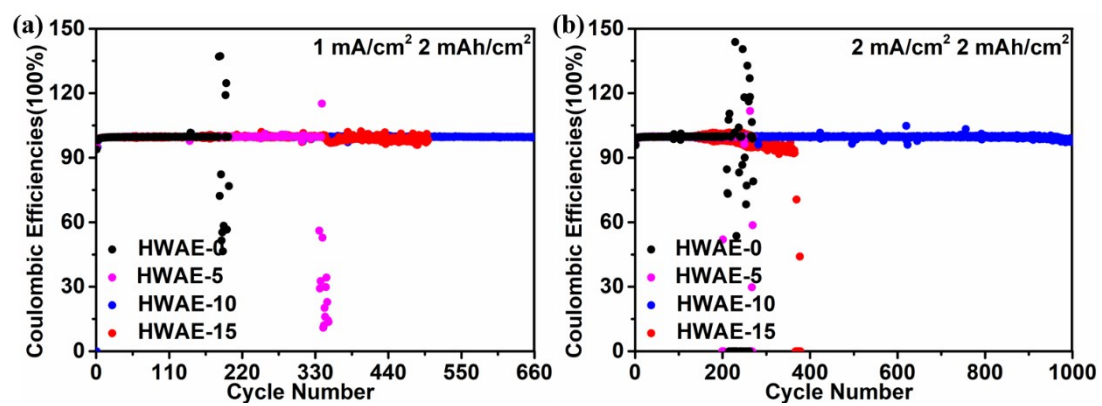


Figure S17. CEs of Zn/Cu cells in HWAEs at (c) 1 mA/cm² and (e) 2 mA/cm² with a cycling capacity of 2 mAh/cm².

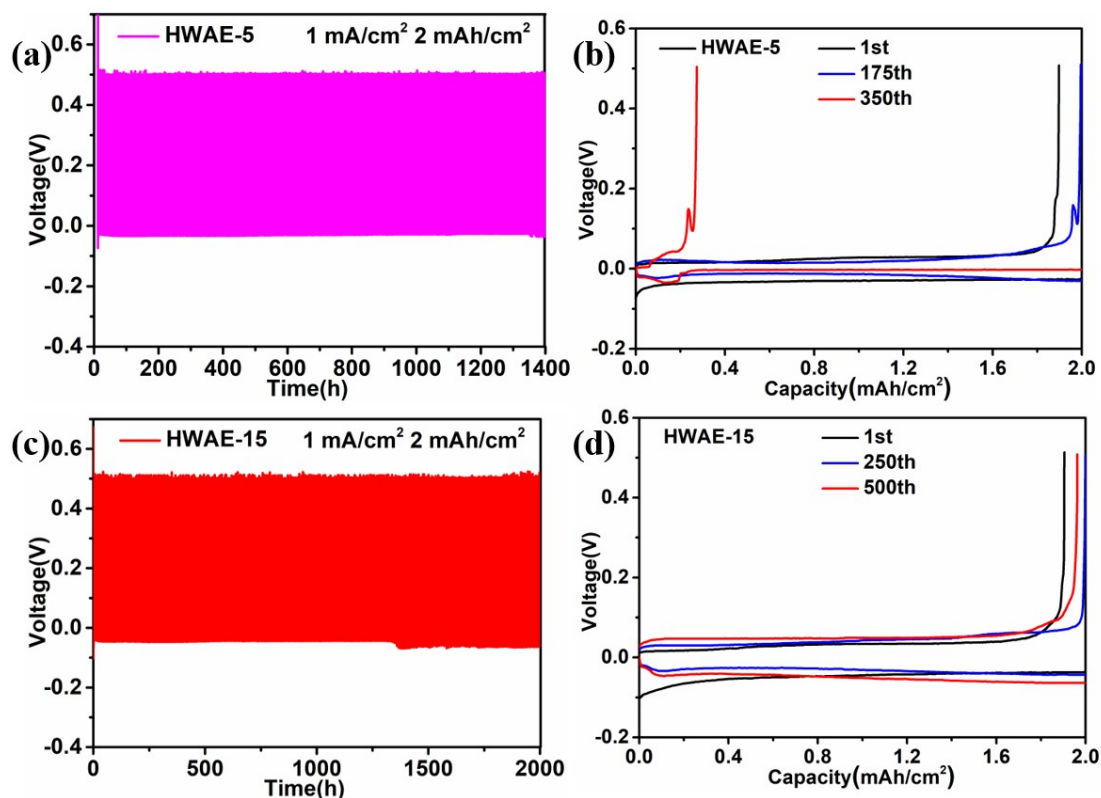


Figure S18. Time-voltage curves of CE in (a) HWAE-5 and (c) HWAE-15 at 1 mA/cm² with a cycling capacity of 2 mAh/cm²; Corresponding detailed deposition/stripping voltage curves in (b) HWAE-0 and (d) HWAE-15 at 1 mA/cm² with a cycling capacity of 2 mAh/cm².

It is found that the stripping capacity is larger than the deposition capacity in HWAE-5.

This is caused by the short circuit from Zn dendrites.

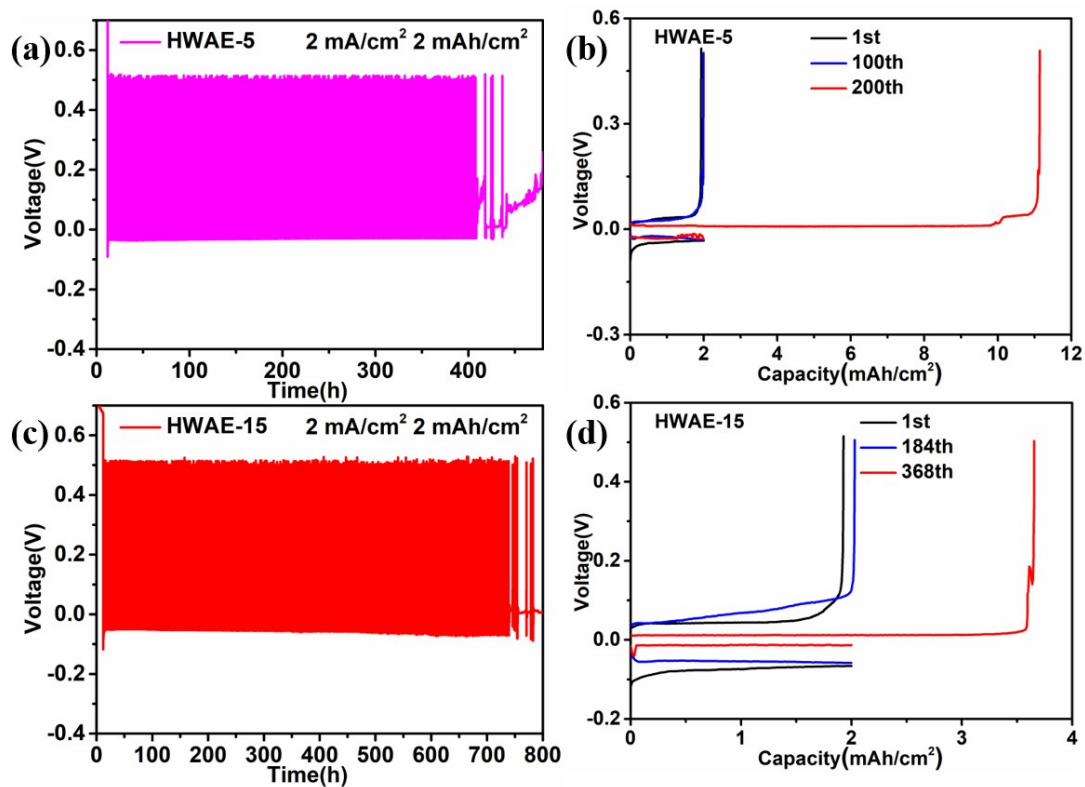


Figure S19. Time-voltage curves of CE in (a) HWAE-5 and (c) HWAE-15 at 2 mA/cm² with a cycling capacity of 2 mAh/cm²; Corresponding detailed deposition/stripping voltage curves in (b) and (d) HWAE-15 at 2 mA/cm² with a cycling capacity of 2 mAh/cm².

It is found that the stripping capacity is larger than the deposition capacity in HWAE-5 and HWAE-15. This is caused by the short circuit from Zn dendrites.

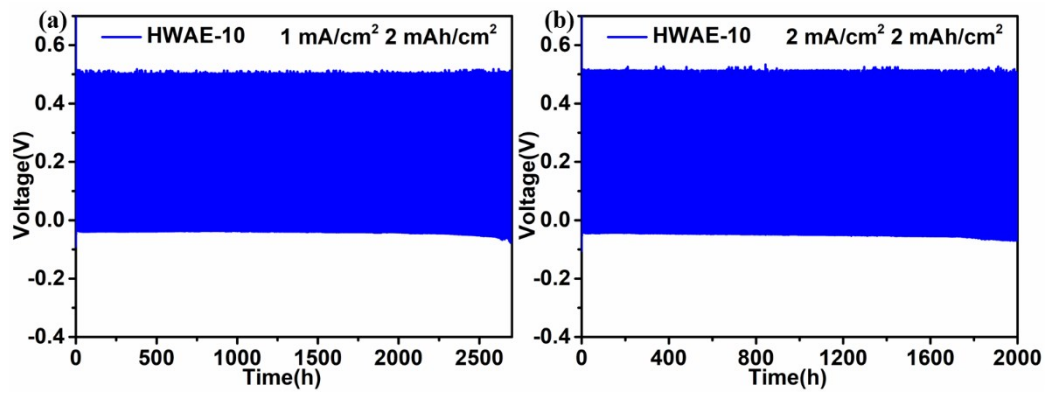


Figure S20. Time-voltage curves of CE in HWAE-10 at (a) 1 mA/cm² and (b) 2 mA/cm² with a cycling capacity of 2 mAh/cm².

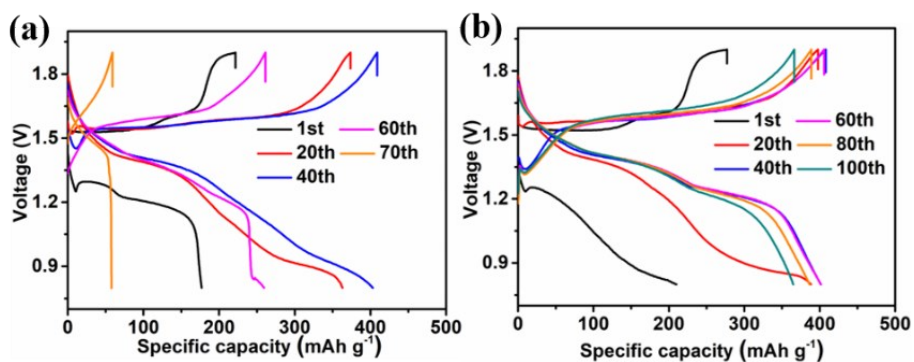


Figure S21. Charge/discharge profiles of Zn/Cu cells at 300 mA/g in HWAE-0 and HWAE-10, with N:P ratios of 10:1.

The full cell displays much better capacity retention in HWAE-10 compared that in HWAE-0. A discharge capacity of 364.1 mA g⁻¹ is maintained after 100 cycles in HWAE-10, corresponding to the capacity retention of ~90%. By contrast, the full cell only has a discharge capacity of 52.8 mA g⁻¹ after 70 cycles in HWAE-0. The stable cycling performance of the full cells verifies the compatibility of AN additive to the cathode. It is worth noting that the full cells show different discharge profiles at the first cycle in HWAE-0 and HWAE-10. This phenomenon may be attributed to the slow electrochemical reaction caused by high desolvation energy in HWAE-10.

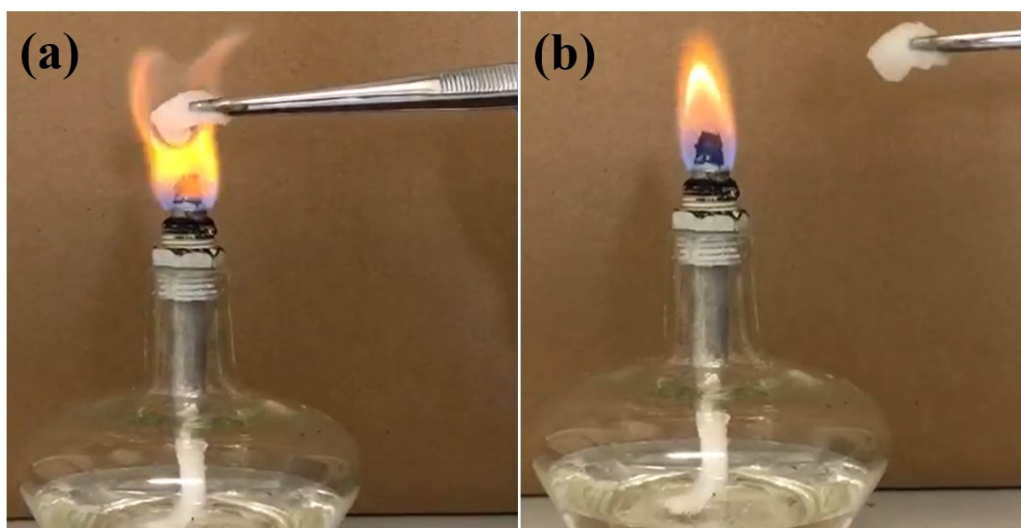


Figure S22. Flammability test for the HWAE-10 with (a) the flame source and (b) after heating, respectively.

Table S1 Reduction and oxidation potentials in 0.1 M ZnSO₄ with/without AN

Electrolytes	V _{deposition} (V)	V _{stripping} (V)
0.1 M ZnSO ₄	-1.45	-0.66
0.1 M ZnSO ₄ with 5% AN	-1.48	-0.68
0.1 M ZnSO ₄ with 10% AN	-1.51	-0.71
0.1 M ZnSO ₄ with 15% AN	-1.53	-0.73

For oxidation process, a negative shift of the oxidation potential is observed upon adding AN into 0.1 M ZnSO₄ (Figure 2a), suggesting the Zn stripping is more likely to occur in hybrid water/AN electrolytes, which is consistent with the function of complexing agent.^[1]

Reference

1. M. Kim, D. Yun, J. Jeon, J. Power Sources, 2019, **438**, 227020.